38

8 TWO-DIMENSIONAL NMR SPECTROSCOPY

AD BAX

CONTENTS

I. INTRODUCTION

When Ernst and Anderson (mation of pulse responses, t significantly and allowed the recorded routinely. Broad-ban the experiment to obtain the s removed and sensitivity enh Numerous experimental schen information from ^{13}C nmr da data, measurement of heteror exchange, and determination of which proton resonance an coupled nuclei.

It was 1971 when Jeener[1(transformation in nmr spectro the generality of the concept oldest two-dimensional ^{13}C e methods,[12–16] which are desc multiplets is effectively remov chemical shifts along one of t ture along the other axis of the determination of the heteronu protons directly coupled to the for those experiments are cohe tion,[17] multiplicity selective e Shortly after the introduction new experiments was propose lated with which proton reson ^{13}C nucleus.[25–32] Of this collec II. It appears that these so-call use once they have been set u very simple to interpret and conventional one-dimensional or INDOR.[8]

More recently a set of two- by Ernst and co-workers[33–37] to exchange. Those experiments ^{13}C, for the proton-decoupled nances, each representing a ce nances are split by homonucle analysis. These experiments are

220
221
222
226
Samples 227
228
229
231
231
231
232

I. INTRODUCTION

When Ernst and Anderson (1) introduced the application of Fourier transformation of pulse responses, this improved the sensitivity of nmr spectroscopy significantly and allowed the ^{13}C spectra of many organic compounds to be recorded routinely. Broad-band proton decoupling[2–6] is usually used throughtout the experiment to obtain the simplest spectrum, with all proton-carbon splittings removed and sensitivity enhanced by the nuclear Overhauser effect (NOE).[7] Numerous experimental schemes have been developed later to extract valuable information from ^{13}C nmr data. These include the measurement of relaxation data, measurement of heteronuclear coupling constants, detection of chemical exchange, and determination by means of the double resonance[3,8,9] techniques of which proton resonance and which carbon resonance correspond to directly coupled nuclei.

It was 1971 when Jeener[10] introduced the idea of two-dimensional Fourier transformation in nmr spectroscopy, and it was a number of years later before the generality of the concept was pointed out by Aue et al.[11] Historically the oldest two-dimensional ^{13}C experiments are the two-dimensional *J*-resolved methods,[12–16] which are described in Section III. Overlap of ^{1}H-coupled ^{13}C multiplets is effectively removed in these experiments by mapping out the ^{13}C chemical shifts along one of the frequency axes and the ^{1}H-^{13}C multiplet structure along the other axis of the two-dimensional spectrum, allowing an accurate determination of the heteronuclear coupling constants and of the number of protons directly coupled to the ^{13}C site considered. One-dimensional alternatives for those experiments are coherent off-resonance decoupling,[3] selective excitation,[17] multiplicity selective experiments,[18–23] or simply isotope substitution.[24] Shortly after the introduction of the *J*-resolved methods, a whole avalanche of new experiments was proposed to determine which carbon resonance is correlated with which proton resonance, that is, which proton is coupled to which ^{13}C nucleus.[25–32] Of this collection, the most useful ones are treated in Section II. It appears that these so-called shift correlation experiments are very easy to use once they have been set up for the first time, and the resulting spectra are very simple to interpret and generally give much better sensitivity than the conventional one-dimensional alternatives: selective heteronuclear decoupling or INDOR.[8]

More recently a set of two-dimensional nmr experiments has been proposed by Ernst and co-workers[33–37] to determine the presence and the rate of chemical exchange. Those experiments are often conveniently performed by detecting ^{13}C, for the proton-decoupled ^{13}C spectrum consists of a set of isolated resonances, each representing a certain site in the molecule, whereas proton resonances are split by homonuclear coupling, which complicates the quantitative analysis. These experiments are the two-dimensional alternative for the conven-

tional one-dimensional experiments in which a single resonance is inverted.[38–40] For more information about those experiments the reader is referred to the literature.[33–37]

Another set of experiments, recently proposed, has the purpose of detecting homonuclear ^{13}C coupling in natural abundance samples.[41–48] These experiments appear to be useful not only to determine the size of the coupling constants but also to determine which carbons are directly coupled, allowing an unambiguous and straightforward assignment of the ^{13}C spectrum and in some cases even the complete reconstruction of the carbon skeleton of unknown compounds. These experiments are briefly discussed in Section IV.

Furthermore, the development of two-dimensional nmr has catalyzed the evolution of a large number of one-dimensional experiments such as the INEPT,[49–50] INADEQUATE,[41] and DEPT[22] experiments, which are essentially offshoots from two-dimensional nmr experiments.

Although the inexperienced reader might find the *J* spectroscopy experiments, discussed in Section III, easier to understand than the various heteronuclear shift correlation experiments, the latter are treated first because of their fundamental nature and their practical importance.

II. CORRELATION OF PROTON AND CARBON CHEMICAL SHIFTS

Heteronuclear chemical shift correlation spectroscopy probably is the most important class of two-dimensional ^{13}C experiments. The experiments are suitable for routine use and demand only simple and limited operator interaction. If they are performed properly, the sensitivity of the heteronuclear shift correlation experiments is rather good, and only a factor of 3 to 5 less than with a conventional ^{13}C proton-decoupled experiment. The information one gets with these experiments is the resonance frequency of the proton(s) coupled directly (or long range) to the various ^{13}C nuclei in the molecule. The experiments can all be understood using simple physical vector pictures and they are treated in detail.

A large variety of heteronuclear chemical shift correlation experiments exists.[25–32,51,52] Not all of those are treated here, but an attempt is made to present some experiments in a way that is easy to understand and gives a useful insight into the general fundamentals of two-dimensional correlation spectroscopy.

A. The Basic Experiment

For simplicity, first a single ^{13}C nucleus bonded to an isolated proton is considered; the appropriate energy level diagram is shown in Figure 8.1*a*. The deviation of the average populations of these energy levels at Boltzmann equilibrium can be represented by the large numbers shown in the diagram. The longitudinal magnetization for a certain transition is directly proportional to the difference

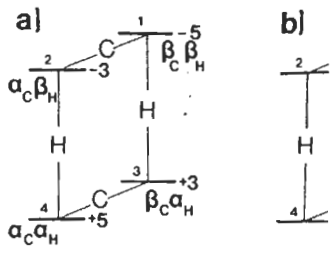

in the population of the corr
numbers given in Figure 8.1*a*
doublet components are both
of the two proton transitions,
then the new populations sh
magnetizations for the two ^{13}
the changes in longitudinal ^{1}
The magnitude of these chang
ton magnetization present bef
longitudinal magnetization th
populations of the other prot
changes in the longitudinal ma
have been $+8$ and -8, respe
proton resonances are inverte
occurs. Hence it is the differe
determines the change in ^{13}C r

The basic two-dimensional
differential proton spin inversi
applied along the x axis of the
8.2). In Figure 8.3 the evolut
during this $90°_x$–t_1–$90°_x$ seque
the second proton pulse, the lo
to $-\cos(\Omega_H + \pi J)t_1$ and $-$co
offset due to the chemical shi
in longitudinal ^{13}C magnetizat

$$\Delta I_1 = \cos($$

$$\Delta I_2 = \cos($$

for the two ^{13}C doublet compon
^{13}C magnetization are observe
second proton pulse (Figure 8

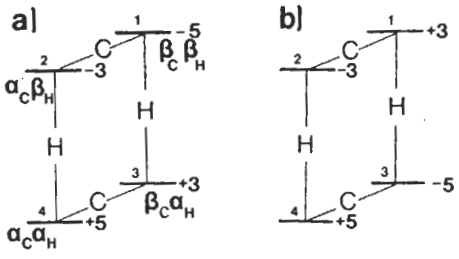

Figure 8.1
The energy level diagram for a ^{13}C-^{1}H spin system with the deviations of the average population in *(a)* thermal equilibrium and *(b)* after selective inversion of proton transition 1–3. Large numbers specify the deviations from the average population of the energy levels. Small numbers simply index the states.

in the population of the corresponding energy levels; that is, in terms of the numbers given in Figure 8.1*a*, the longitudinal magnetizations for the two ^{13}C doublet components are both +2. If a population inversion is created across one of the two proton transitions, without significantly affecting the other transition, then the new populations shown in Figure 8.1*b* apply. Now the longitudinal magnetizations for the two ^{13}C doublet components are −6 and +10; that is, the changes in longitudinal ^{13}C magnetization are −8 and +8, respectively. The magnitude of these changes is directly proportional to the longitudinal proton magnetization present before the selective inversion. Hence it is the proton longitudinal magnetization that is being transferred to the ^{13}C nuclei. If the populations of the other proton resonance had been selectively inverted, the changes in the longitudinal magnetizations of the ^{13}C doublet components would have been +8 and −8, respectively. Similarly, it is easily seen that if both the proton resonances are inverted, no change in longitudinal ^{13}C magnetization occurs. Hence it is the difference in inversion of the two proton resonance that determines the change in ^{13}C magnetizations.

The basic two-dimensional chemical shift correlation experiment includes a differential proton spin inversion. This is accomplished by two 90° proton pulses applied along the x axis of the rotating frame and separated by a time t_1 (Figure 8.2). In Figure 8.3 the evolution of the two proton magnetization components during this $90°_x$–t_1–$90°_x$ sequence is shown for a specific value of t_1. Just after the second proton pulse, the longitudinal proton magnetizations are proportional to $-\cos(\Omega_H+\pi J)t_1$ and $-\cos(\Omega_H-\pi J)t_1$, where Ω_H is the proton frequency offset due to the chemical shift and J the C-H coupling constant. The changes in longitudinal ^{13}C magnetizations, ΔI_1 and ΔI_2, are thus proportional to

$$\Delta I_1 = \cos(\Omega_H+\pi J)t_1 - \cos(\Omega_H-\pi J)t_1 \tag{1a}$$

$$\Delta I_2 = \cos(\Omega_H-\pi J)t_1 - \cos(\Omega+\pi J)t_1 \tag{1b}$$

for the two ^{13}C doublet components, respectively. These changes in longitudinal ^{13}C magnetization are observed by the application of a 90° ^{13}C pulse after the second proton pulse (Figure 8.2). Figure 8.4 shows a series of ^{13}C spectra

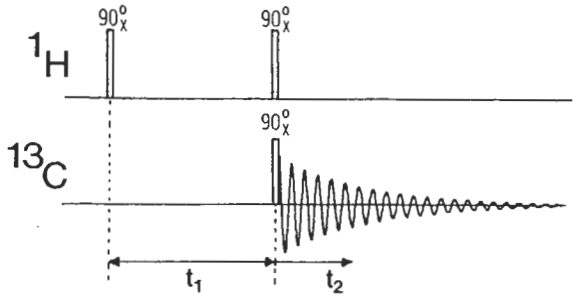

Figure 8.2
Pulse scheme of the basic heteronuclear shift correlation experiment.

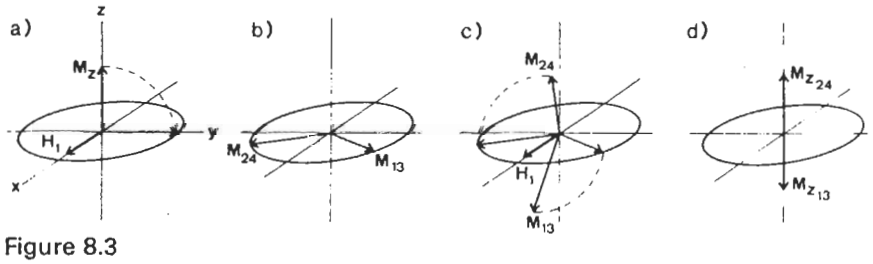

Figure 8.3
The evolution of proton doublet magnetization vectors during a $90°_x$–t_1–$90°_x$ pulse sequence applied to the protons.

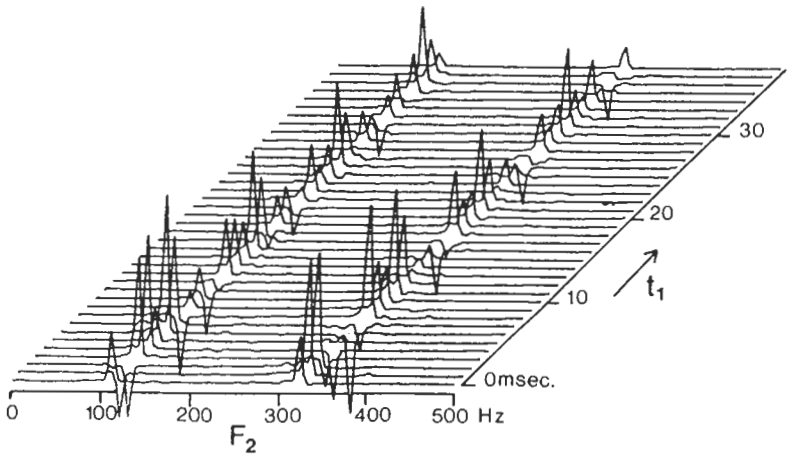

Figure 8.4
A set of proton-coupled ^{13}C spectra of chloroform, obtained with the sequence of Figure 8.2 for incrementing values of t_1.

obtained with the sequ
values of the length o
the amplitudes of the
amplitude with the pr
there is always the
doublet components,
ulated component.

If one now takes cr
to the t_1 axis, the se
resonance frequencies
transformation of such
intensities at F_1 freque
unmodulated Boltzma
Fourier transformation
sections parallel to the
the two-dimensional s

B. Heteronuclear

For chemical shift cor
ent in Figure 8.5, is a
during both time inte
from each other. Duri

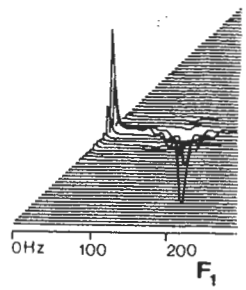

Figure 8.5
Heteronuclear shift corr
ent in both dimensions.

obtained with the sequence of Figure 8.2 on a sample of chloroform, for different values of the length of the evolution period, t_1. As can be seen from this figure, the amplitudes of the two ^{13}C doublet components are clearly modulated in amplitude with the proton frequencies, and in opposite manner. On top of that, there is always the ^{13}C Boltzmann magnetization, which is positive for both doublet components, and a factor of 4 smaller than the magnitude of the modulated component.

If one now takes cross sections through the data matrix of Figure 8.4, parallel to the t_1 axis, the sections taken at F_2 frequencies corresponding to the ^{13}C resonance frequencies show the modulation as given in Equation 1. Fourier transformation of such a cross section yields two resonance lines with opposite intensities at F_1 frequencies equal to $(\Omega_H + \pi J)$ and $(\Omega_H - \pi J)$. The constant, unmodulated Boltzmann component gives rise to a zero-frequency peak after Fourier transformation with respect to t_1. Fourier transformation of all the cross sections parallel to the t_1 axis then, after transposition of the data matrix, gives the two-dimensional spectrum shown in Figure 8.5.

B. Heteronuclear Decoupling in Both Frequency Dimensions

For chemical shift correlation, the two-dimensional multiplet structure, as present in Figure 8.5, is an unnecessary complication, and therefore it is better if during both time intervals t_1 and t_2 the protons and ^{13}C nuclei are decoupled from each other. During the evolution period this is most easily achieved by the

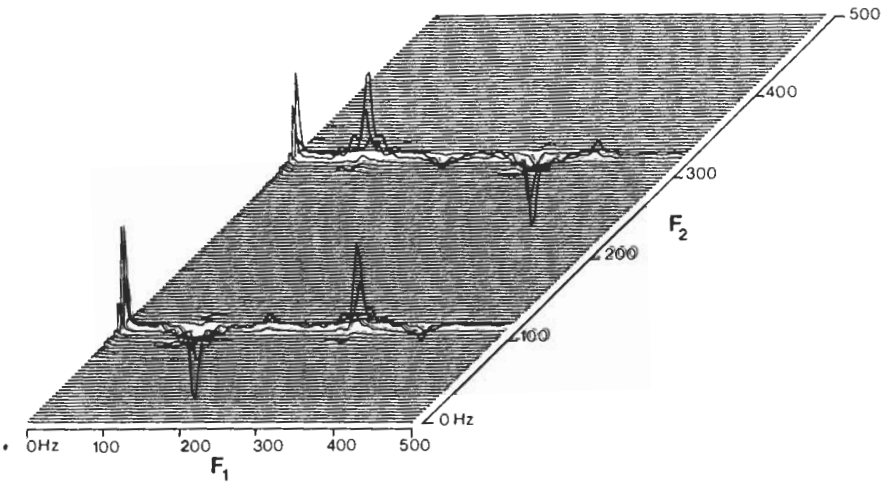

Figure 8.5
Heteronuclear shift correlation spectrum of chloroform with heteronuclear coupling present in both dimensions.

application of a 180° ^{13}C pulse at the midpoint of the evolution period, t_1 (Figure 8.6). This has the effect that the two proton magnetization vectors, corresponding to the ^{13}C in the α and in the β states, respectively, interchange their frequencies at this point, since the ^{13}C nucleus is flipped to the opposite spin state. As a consequence, at the end of the evolution period, t_1, both proton doublet components have the same phase in the transverse plane. As pointed out before, it is the difference in inversion of the two proton doublet components that determines the transfer of magnetization to the ^{13}C nucleus. This difference is maximized if the two proton doublet components have opposite phases, and therefore an extra delay, Δ_1, with fixed length $1/2J$, is inserted before the second proton pulse is applied.[26]

Proton decoupling during the detection period cannot be started immediately after the ^{13}C observe pulse, because the ^{13}C doublet components (or the triplet or quartet components in the case of a CH_2 or a CH_3 group) are in antiphase at this point in time as the amplitudes are modulated in an opposite fashion. However, if a delay with fixed length, Δ_2, is inserted (Figure 8.6) before the proton broad-band decoupling is started, the ^{13}C multiplet components generally have a net resultant at the end of this interval, and no mutual cancellation occurs. In Figure 8.7 the magnitude of the vector sum of the ^{13}C multiplet components as a function of the time, Δ_2, is shown for a CH group, a CH_2 group, and a CH_3 group. It can be seen from Figure 8.7 that, if a value of $0.3/J$ is selected for the duration of Δ_2, good intensities are observed for methine, methylene, and methyl sites. Note that for optimization of the duration of the interval, Δ_1, we are always dealing with a proton doublet due to the ^{13}C splitting, and a value $1/2J$ is optimum for Δ_1 in all cases.

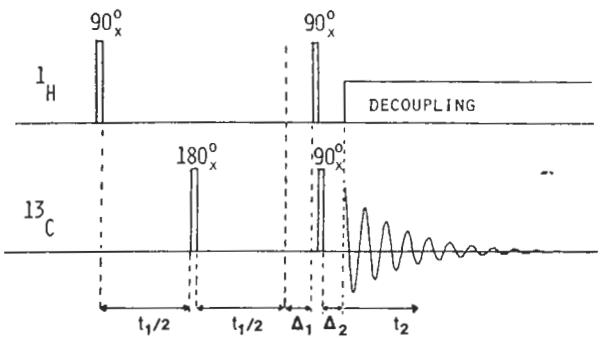

Figure 8.6
Scheme of the heteronuclear shift correlation experiment with heteronuclear decoupling during both the evolution and detection periods. In its simplest form all pulses are applied along the x axis. Selecting the phases given in Table 8.1 for the various steps provides suppression of axial peaks and determination of the sign of the proton frequency.

II. Co

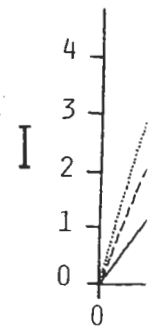

Figure 8.7
The Δ_2 dependence of the
(Figure 8.6) for a methin
(dotted line). Intensity 1 c
rium.

C. Suppression of A

The spectrum of Figure
Those peaks carry only r
ing two experiments for
8.6 and one with the s
modulation of the ^{13}C i
contributing to the axial
the data acquired in one
periment causes cancella

As the ^{13}C signal is
possible to determine wh
that is, whether the moc
of the ^{1}H transmitter freq
the cosine component of
Equation 1. If an experi
the y axis were perform
would be transferred to
dimensional quadrature
then be determined, if th
each value of t_1, the sec
shows the various phase
in the experiment. Of co
phase cycling scheme in
spectrometer; a 90° incr

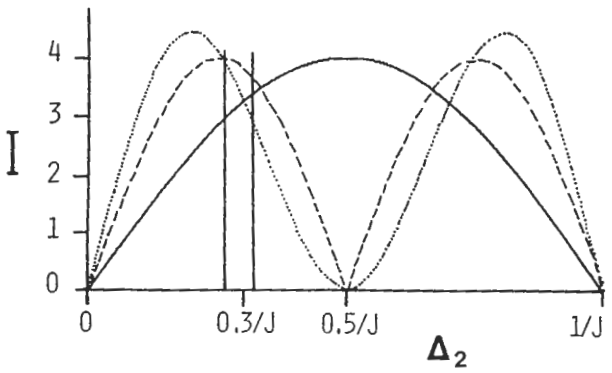

Figure 8.7
The Δ_2 dependence of the ^{13}C amplitude in the decoupled shift correlation experiment (Figure 8.6) for a methine (solid line), a methylene (broken line), and a methyl site (dotted line). Intensity 1 corresponds to the total ^{13}C magnetization in thermal equilibrium.

C. Suppression of Axial Peaks and Quadrature ^1H Detection

The spectrum of Figure 8.5 shows so-called axial peaks at $F_1 = 0$ frequency. Those peaks carry only redundant information, and can be removed by performing two experiments for each value of t_1, one as given in Figure 8.2 or Figure 8.6 and one with the second proton pulse applied along the $-x$ axis. The modulation of the ^{13}C is opposite in the two experiments, whereas the signal contributing to the axial peaks is identical in the two steps. Thus subtraction of the data acquired in one experiment from the data acquired in the second experiment causes cancellation of the unmodulated components.

As the ^{13}C signal is modulated in amplitude (not phase), it is not directly possible to determine whether the modulation frequency is positive or negative, that is, whether the modulation frequency is at the low field or high field side of the ^1H transmitter frequency. This amplitude modulation occurs because only the cosine component of the ^1H magnetization is measured, as can be seen in Equation 1. If an experiment with the phase of the second proton pulse along the y axis were performed, the sine component of the proton magnetization would be transferred to the ^{13}C nuclei. As in the case of the conventional one-dimensional quadrature detection, the sign of the modulation frequency could then be determined, if the signals were combined in a proper fashion.[31,54] For each value of t_1, the sequence is repeated a multiple of four times. Table 8.1 shows the various phases of the rf pulses and the receiver[55] for these four steps in the experiment. Of course, the spectroscopist has the freedom to change this phase cycling scheme in order to make it easier to implement on a particular spectrometer; a 90° increase in the phase of the ^{13}C observe pulse should be

Table 8.1
Phase of the Second 90° Proton Pulse, ϕ_1, and the Receiver Phase,[55] ψ, in the Four Steps of the Heteronuclear Shift Correlation Experiment with Quadrature Proton Detection, Sketched in Figure 8.6. All Other Pulses are Applied Along the x Axis

Step No.	ϕ_1	Acq. (ψ)
1	x	x
2	y	$-y$
3	$-x$	$-x$
4	$-y$	y

accompanied by a 90° increase in the phase of the receiver. Similarly, if the 90° ^{13}C pulses in steps 2 and 4 were applied along the $-y$ and $+y$ axes, respectively, the receiver phase should be constant in the four steps of the experiment; that is, all data should be co-added. For the proton pulses, only the relative phases of the first and second 90° pulse matter. A more detailed and explicit description of the shift correlation experiment and the phase cycling required is given in Reference 54.

As an example, Figure 8.8*a* shows a typical heteronuclear shift correlation spectrum for the aromatic carbons in 2-acetonaphthone (inset) obtained at 90 MHz on a Nicolet-360 spectrometer. A 1.5*M* solution in acetone-d_6 in a 12 mm sample tube was used, and four experiments were performed for each value of t_1 with the phases of the rf pulses and the receiver[54] cycled as indicated in Table 8.1. The total measuring time for the two-dimensional experiment was 20 min. A 96 × 512 data matrix was acquired, which means that the experiment was performed for 96 different t_1 values, and 512 *complex* data points were acquired for each value of t_1. Because only aromatic carbons were observed, with a C-H coupling of the order of 160 Hz, both delays Δ_1 and Δ_2 were set equal to 3 msec. The t_1 increment was 2 msec, giving a spectral width of ±250 Hz in the F_1 dimension. After Gaussian broadening of the acquired FID's, used in order to avoid truncation, and matrix transposition, the matrix consists of 512 interferograms of 96 complex data points each. After appropriate digital filtering (see Section II.F.9), zero-filling to 128 complex data points, a second Fourier transformation (this one with respect to t_1), and an absolute-value calculation, a two-dimensional spectrum is obtained. A contour plot is shown in Figure 8.8*a*. For reference the conventional proton spectrum and the proton-decoupled ^{13}C spectrum are shown along the two axes of the two-dimensional spectrum. Figure 8.8*b* shows cross sections through the data matrix at the various ^{13}C chemical shift frequencies, phased individually to the absorption mode. As is clearly

visible in these spectra, the p
proton splitting pattern. Som
assignment of the various reso
care should be taken in interpr
^{13}C satellites in the proton spe

The noise in the cross sec
noise, and would increase if a
is due to instabilities in the
magnetic field homogeneity, s
ature, and small changes in t
common phenomenon in two-
solutions are used. Furtherm
peaks just next to the main pe
the proton trace of C-1, are s
stronger in the proton than in
respect to the center of the spe
imperfections in the F_1 quadrat
shifts in the proton transmitter
by further phase cycling as d
the four step sequence as give
cases, provided that the rf phas
adjusted.

The application of this het
is not limited to small organic
shift correlation spectra of a
appeared in the literature. In b
field (200 MHz) spectrometers
and resolution can be expecte
with a high magnetic field stre

D. Correlation via Long-F

The reason that, in the spectr
directly bonded protons and ^{13}
plings are large enough to caus
during the delay Δ_1 and to cr
phase ^{13}C multiplet component
for the delays Δ_1 and Δ_2 are s
will appear in the final two-di
dimensional shift correlation s
8.8, with the same pulse seque
to 45 and 30 msec, respective

visible in these spectra, the proton resonances show the conventional proton-proton splitting pattern. Sometimes this can be fruitfully used as an aid in assignment of the various resonances, although, as is explained in Section II.E, care should be taken in interpreting the multiplet structure in the case where the ^{13}C satellites in the proton spectrum are strongly coupled.

The noise in the cross section shown in Figure 8.8 is mainly so-called t_1 noise, and would increase if a stronger sample solution were used. This noise is due to instabilities in the spectrometer system, such as small changes in magnetic field homogeneity, small variations in the lock system or in temperature, and small changes in the rf phases and amplitudes. This t_1 noise is a common phenomenon in two-dimensional spectroscopy whenever concentrated solutions are used. Furthermore, some small spurious peaks are visible; the peaks just next to the main peaks on the various traces, most clearly visible in the proton trace of C-1, are spinning side bands which are, of course, much stronger in the proton than in the carbon dimension. Small mirror images with respect to the center of the spectra in Figure 8.8 are also visible, attributable to imperfections in the F_1 quadrature detection. This is due to nonperfect 90° phase shifts in the proton transmitter channel, and can, to a large extent, be eliminated by further phase cycling as described in Section II.F.1. In practice, however, the four step sequence as given in Table 8.1 will suffice in almost all practical cases, provided that the rf phase shifting hardware of the spectrometer is properly adjusted.

The application of this heteronuclear chemical shift correlation experiment is not limited to small organic molecules. Impressive examples of heteronuclear shift correlation spectra of a large peptide[56] and even a small protein[57] have appeared in the literature. In both cases those spectra were recorded on medium-field (200 MHz) spectrometers and a significant improvement in both sensitivity and resolution can be expected if experiments are performed on a spectrometer with a high magnetic field strength.

D. Correlation via Long-Range Couplings

The reason that, in the spectra of Figure 8.8, only the correlations between directly bonded protons and ^{13}C nuclei are visible, is that only those C-H couplings are large enough to cause significant antiphase proton doublet components during the delay Δ_1 and to create in-phase components from the initially antiphase ^{13}C multiplet components during the delay, Δ_2. However, if larger values for the delays Δ_1 and Δ_2 are selected, correlation via long-range couplings also will appear in the final two-dimensional spectrum. Figure 8.9 shows the two-dimensional shift correlation spectrum obtained from the same sample as Figure 8.8, with the same pulse sequence, but with the delays Δ_1 and Δ_2 now adjusted to 45 and 30 msec, respectively. The spectrum has been computed from a 64

× 512 data matrix, and shows correlation for most long-range couplings larger than about 5 Hz. In combination with the spectra of Figure 8.8, this now allows the complete and unambiguous assignment of all the proton and aromatic carbon resonances, including those of the unsubstituted carbons. Unsubstituted carbon C-2 is easily recognized, because it is the only carbon showing a long-range coupling with the methyl protons, folded several times along the F_1 axis, and indicated here with an asterisk. The two other unsubstituted resonances are easily assigned using the knowledge that three bond C-H couplings around an aromatic ring are of the order of 6 Hz, and thus show a long-range correlation peak.

The sensitivity of the long-range coupling correlation experiment is significantly lower than for the direct coupling correlation experiment, in practice a factor of 3 or more. Correlations via direct C-H coupling do not show up in this experiment, if one (or both) of the delays Δ_1 and Δ_2 is equal to an integer number (n) times the reciprocal of the direct coupling constant, n/J, because in this case no net magnetization is transferred. The choice of the duration of the delays Δ_1 and Δ_2 is not as straightforward as in the direct coupling experiment. It depends on how many protons have a significant long-range coupling to a certain ^{13}C and on the magnitudes of those couplings, as well as on the complexity of the proton-proton multiplet structure and on the transverse proton

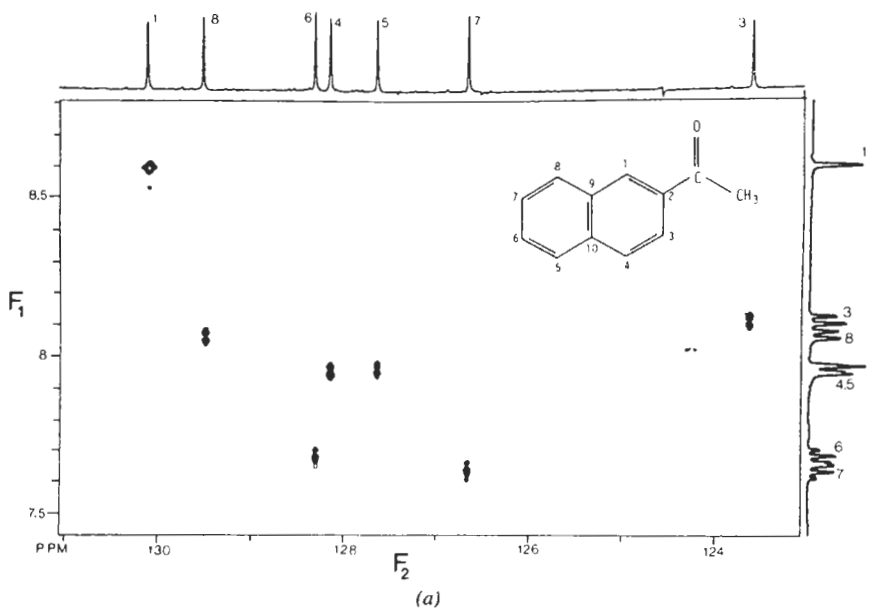

(a)

Figure 8.8
Heteronuclear shift correlation spectra of the protonated aromatic region in 2-acetonaphthone. *(a)* a contour absolute value mode display.

II. C

relaxation time. Usual
where J is now the lor
after the long delay, Δ
the transverse plane, r
magnetization possibly
delay Δ_2 before decou
for Δ_1 are between 25

E. The Effect of St

In the description of th
(Section II.B) proton-p
that if the coupling ar

Figure 8.8 (*Continued*)
(b) Phase-sensitive absor
the two-dimensional spec
frequency.

relaxation time. Usually, values for Δ_1 and Δ_2 that are much shorter than $1/2J$, where J is now the long range C-H coupling constant, must be selected. If not, after the long delay, Δ_1, no proton transverse magnetization will be present in the transverse plane, ready for transfer by the second proton pulse; all proton magnetization possibly transferred to the ^{13}C will have dephased during the delay Δ_2 before decoupling and acquisition are started. Typical optimum values for Δ_1 are between 25 and 80 msec and for Δ_2 between 20 and 50 msec.

E. The Effect of Strong Coupling among the Protons

In the description of the two-dimensional decoupled shift correlation experiment (Section II.B) proton-proton interactions were not taken into account. It appears that if the coupling among the protons[58] is weak, there is no significant dis-

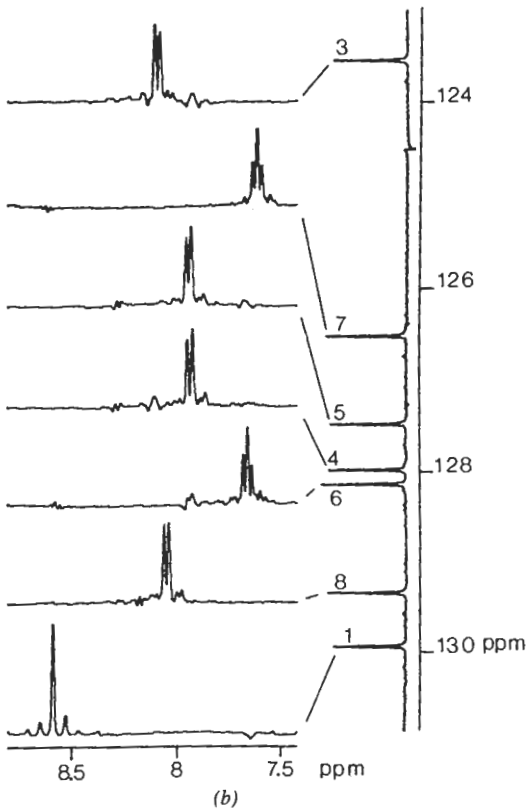

Figure 8.8 (*Continued*)
(b) Phase-sensitive absorption mode cross sections taken parallel to the F_1 axis through the two-dimensional spectrum. The spectrum has been recorded at a 360 MHz proton frequency.

^{13}C decoupling during this interval. In favorable cases this ^{13}C decoupling has become feasible by the development of composite pulse decoupling,[5] which gives decoupling over a wider frequency range than conventional noise or square wave modulated decoupling methods.

F. The Experimental Procedure

The heteronuclear shift correlation experiment appears to be very powerful in solving practical problems. However, at first sight, the execution of this experiment is considerably more complicated than that of the conventional double resonance experiments. In this section a number of points are mentioned that demand attention from the inexperienced two-dimensional operator. The advice given below is of a general nature, and in particular cases better results may be obtained if certain parameters are chosen differently.

1. The Pulse Sequence

The pulse sequence of Figure 8.6 is most commonly used, with the phase cycling of rf pulses and receiver[55] as given in Table 8.1. On some spectrometers the proton decoupling and/or the carbon rf phases are poorly calibrated, which leads to (small) mirror image signals with respect to zero frequency in the F_1 dimension and to a spurious peak at zero frequency for those F_1 traces that carry signal. Those spurious signals can be suppressed by performing four experiments for each step in Table 8.1, incrementing the phases of all proton and carbon pulses, as well as the receiver phase, by 90° each time. This is analogous to the CYCLOPS[62] cycling, used in conventional one-dimensional experiments.

2. Delay Δ_1

Because most direct C-H coupling constants are in the range of 125–170 Hz, a delay Δ_1 equal to 3.3 msec is close to optimum in most cases. If the experiment is performed for the purpose of detecting long-range connectivity, the delay Δ_1 is chosen much longer. If the proton spectrum has a very complex multiplet structure or very short transverse relaxation times, the delay Δ_1 is set to a value of the order of 25 msec. If the proton multiplet structure is not resolved, but consists of a number of overlapping lines and has a width of P Hz, the delay Δ_1 should always be shorter than $1/(2P)$ sec. For well-resolved or narrow proton multiplet structures, the duration of Δ_2 can be chosen as long as 100 msec, but, of course, not larger than $1/(2J)$, if J is the expected value for the long-range coupling.

3. Delay Δ_2

As discussed in Section II.B, the optimum length of Δ_2 is different for CH, CH_2, and CH_3 groups. A value of 2 msec usually shows all correlations with fair intensity. However, if only the methyl or aromatic region of a ^{13}C spectrum

is detected, for instance, the duration of Δ_2 would be set to 1.6 and 3.0 msec, respectively.

For detection of long-range connectivity, the delay would be set to a value of the order of 20 to 50 msec, now depending on the complexity of the long-range ^{13}C multiplet structure.

4. Experiment Delay Time

Because the magnetization is transferred from protons to ^{13}C, the optimum length of the delay time (T) between the end of acquisition and the first proton pulse of the next experiment depends on the longitudinal relaxation time (T_1) of the protons, rather than on the usually much longer T_1's of the ^{13}C nuclei. It can be shown that a delay time $T = 1.3T_1$ gives optimum sensitivity.[63] Care has to be taken that during this delay time, T, no rf power from the decoupling transmitter, which has a frequency near the proton spectrum, leaks through to the decoupling coil, because this will cause (partial) saturation of the protons, degrading sensitivity.

5. Acquisition Times

In the case of poor sensitivity, the sampling time along the t_2 axis should be at least equal to the decay constant T_2 of the ^{13}C signal, in order to avoid sensitivity loss. The length of the acquisition time along the t_1 axis, which equals the number of increments times the length of the t_1 increment, depends on the ^1H resolution required, the amount of data storage available, and the sensitivity. One should realize that resolution of the proton multiplet structure in the F_1 dimension is hardly ever necessary, whereas it increases the number of resonances in the two-dimensional spectrum and therefore decreases the sensitivity. In many cases a 50–100 msec acquisition time in the t_1 dimension is sufficient, unless high resolution of the proton spectrum is absolutely necessary.

6. Acquisition Frequency in the t_1 Dimension

In order to avoid folding, the effective acquisition frequency in the t_1 dimension, which is equal to the reciprocal of the t_1 increment, must be higher than twice the maximum offset frequency from the ^1H transmitter to a proton resonance of interest. The proton transmitter frequency must be set to the center of the ^1H region of interest in order to minimize the required acquisition frequency and the amount of data storage space required.

7. Calibration of the Proton Pulses

The proton pulses are usually applied by using the proton decoupler in the coherent mode for a short period of time. The calibration of the width of the proton pulses is not very critical, since, as can be derived, the amplitude of the modulation is approximately proportional to $\sin^2(\alpha)$, if proton pulses with flip angle α are applied. Because the strength of the decoupler rf field cannot be determined directly via a 180° calibration (as commonly used for the observe

channel), an indirect a
the reduction in the ^{13}
pling.[3] However, a m
is to apply the sequen
tigation or to a simple
to $1/(2J)$, where J is
ered, no signal for thi
This method is most
although methylene a
pulse is applied, but w
the sensitivity of this
time $1/(2J)$ after the p
coupling scheme used,
that do not correspond
due to heteronuclear m

8. Shimming of th

Because a large sample
spinning side bands mi
neity is four times wor
are visible in the traces
in the nonspinning mod

9. Digital Filtering

Because an absolute val
of the two-dimensional
digital filter be used th
nances. Many different
requirement is that the fi

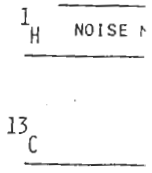

Figure 8.11
Pulse sequence for the calib
flip angle is adjusted to 90°,

channel), an indirect approach has to be chosen. The traditional way is to observe the reduction in the ^{13}C multiplet splitting under coherent off-resonance decoupling.[3] However, a more convenient way for calibrating the flip angle α to 90° is to apply the sequence sketched in Figure 8.11 to the compound under investigation or to a simple test compound. It can be shown[64] that if the delay is set to $1/(2J)$, where J is the direct C-H coupling constant of the multiplet considered, no signal for this carbon is detected if the proton-flip angle α equals 90°. This method is most accurate if a methine carbon is used for the calibration, although methylene and methyl groups also give zero signal if a 90° proton pulse is applied, but with a less sharply defined zero point. In order to improve the sensitivity of this calibration method, proton decoupling can be started at time $1/(2J)$ after the proton pulse. However, depending on the broad-band decoupling scheme used, this can give rise to spurious broad signals at frequencies that do not correspond to conventional ^{13}C resonance frequencies and that are due to heteronuclear multiple quantum coherence.[65]

8. *Shimming of the Magnetic Field*

Because a large sample diameter is usually used for the detection of ^{13}C, proton spinning side bands might occur, since the effect of magnetic field inhomogeneity is four times worse for protons than for ^{13}C. These spinning side bands are visible in the traces shown in Figure 8.8*b*. Careful shimming of the magnet in the nonspinning mode is important to limit the size of these peaks.

9. *Digital Filtering in the* t_1 *Dimension*

Because an absolute value calculation is usually performed before a contour plot of the two-dimensional spectrum is made, it is recommended that some kind of digital filter be used that minimizes the tailing of absolute value mode resonances. Many different filtering functions are well suited to do this: the main requirement is that the filtering function converts the decay function of the signal

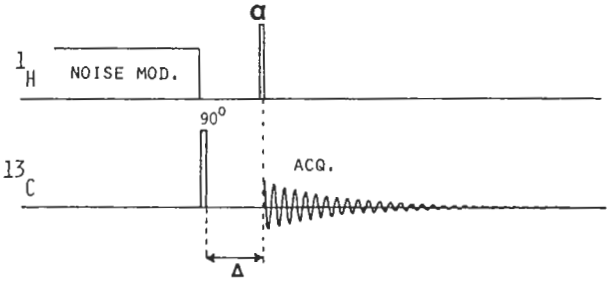

Figure 8.11
Pulse sequence for the calibration of the proton rf field strength. When the proton pulse flip angle is adjusted to 90°, no signal is detected.

into a function that has some similarity to the envelope of a spin echo.[66] An example of such a window is given in Figure 8.12*a*. This function can be approximated in various ways, for example, by the "sine-bell squared" window, the "sine-bell" window,[67] convolution difference filtering,[68] the "pseudo-echo" window,[69] or simply trapezoidal multiplication. However, although the line shape improves by the use of the filter of Figure 8.12*a*, intensity distortions of overlapping resonances occur, and the sensitivity loss due to the use of the filter is often quite large. Therefore it is usually better to use a "compromise filter" with a shape as indicated in Figure 8.12*b*. This filter improves the absolute value mode line shape and does not decrease sensitivity much. This kind of filtering function can be approximated by using suitable parameters in the window functions mentioned above. In the case where phase-sensitive cross sections are displayed, as, for example, in Figure 8.8*b*, it is better to use conventional line narrowing[70] or sensitivity enhancement techniques to get the optimum spectrum.

10. Digital Filtering in the t_2 Dimension

Because resolution of the proton-decoupled ^{13}C spectrum is usually not a major problem, Gaussian or Lorentzian broadening can be used in the t_2 dimension to improve sensitivity or to avoid truncation effects. If sensitivity is no problem, a filter with the shape given in Figure 8.12*b* can be used. If the signals in the t_2 dimension are severely truncated, it is better to use Gaussian than Lorentzian broadening, for this gives relatively better sensitivity and line shapes.

G. Other Shift Correlation Experiments

As mentioned at the beginning of this chapter, many different experimental techniques exist to correlate the chemical shifts of coupled nuclei. In this section some of those techniques not yet discussed are treated very briefly.

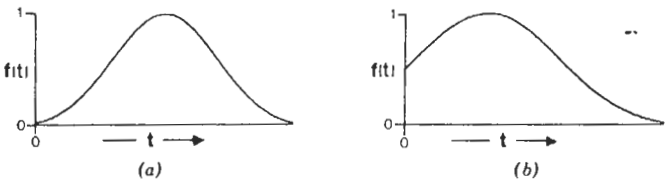

Figure 8.12
Shapes of the filtering functions, $f(t)$, which *(a)* completely suppress absolute-value-mode tailing at high cost in sensitivity, and *(b)* partially suppress absolute-value-mode tailing at low cost in sensitivity.

II. Corr

1. The RELAY Exper

The RELAY experiment, plication by Bolton and B nuclear and heteronuclear ferred from one proton to its directly coupled ^{13}C n be identified, provided tha tual coupling. The experir sensitive version of the o cycling.[72] The sequence is perform the same functio to transfer magnetization 180° ^{13}C pulse, applied at of heteronuclear coupling, described in Section II.B. ponents that have been $-t_1-90^\circ_x$ sequence are initi for a time $1/(2J_{HH})$ before the homonuclear proton c proton magnetization to th clear multiplet component by the application of a 180 magnetization transfer take F_1 dimension, the phases experiment according to T in more detail in Section reference phase.

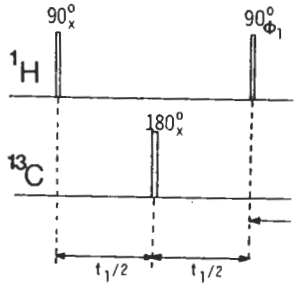

Figure 8.13
Pulse sequence of the RELA of $1/(4J_{HH})$, and the delays Δ

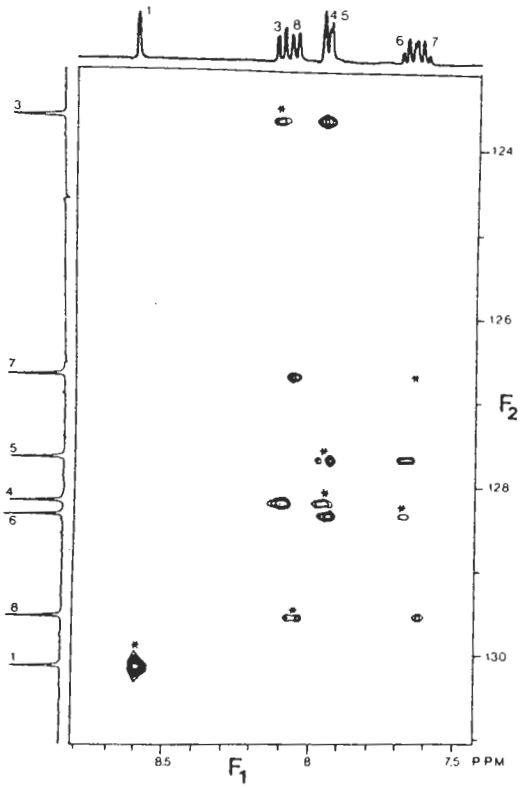

Figure 8.14
RELAY two-dimensional spectrum of the aromatic region in 2-acetonaphthone. The peaks due to direct coupling are indicated with asterisks, as is the position of the resonance due to direct coupling with H7. The other peaks indicate indirect coupling over two bonds.

2. *Indirect Detection of* ^{13}C

In principle, higher sensitivity can be obtained if the sequences discussed in sections II.A–D are applied the reversed way, that is, if the ^{1}H and ^{13}C labels are interchanged in the diagrams of Figures 8.2 and 8.6. In this case protons would be detected during acquisition, which, owing to the higher proton magnetogyric ratio, offers the best sensitivity. In this case, the sequences proposed by Bodenhausen and Ruben[51] and Muller[29] are the most promising. However, it turns out that for ^{13}C the possible gain in sensitivity does not offset the increase in experimental inconvenience.[54] One of the major problems is the suppression of the proton signals that are not directly coupled to a ^{13}C. Hence those experiments are not recommended for general use.

3. *Heteronuclear Chemical Shift Correlation via Multiple Quantum Coherence*

For the correlation of heteronuclei, Bendall et al.[32] proposed an experiment which they claim to be superior and which is very closely related to experiments proposed by Minoretti et al.[30] and Muller.[29] However, they show a different application: simultaneous correlation of chemical shifts and multiplicity determination of the ^{13}C site. The multiplicity determination is based on the different orders of heteronuclear multiple quantum coherences that can be created in CH, CH_2, and CH_3 groups. The number of resonances in the "superior" two-dimensional spectrum increases compared with the normal shift correlation experiment, increasing its complexity and decreasing the sensitivity. Experimental results obtained by Bendall et al.[32] and by me are rather disappointing. This is partly due to the severe effect which static magnetic field inhomogeneity has on the higher orders of heteronuclear multiple quantum coherence[73] and partly to the larger data matrix that is generally required because of the higher modulation frequencies in the t_1 dimension.

It is recommended here that, rather than the "superior" sequence, one use the new one-dimensional experiments[18–23] for multiplicity determination, in combination with the normal heteronuclear shift correlation experiments.

III. *J* SPECTROSCOPY

As mentioned in the introduction, heteronuclear *J* spectroscopy was the first class of two-dimensional experiments to receive widespread attention. The main advantage of using two-dimensional heteronuclear *J* spectroscopy is that overlapping multiplets can easily be unraveled by mapping out the C-H multiplet splitting in the F_1 frequency dimension and the proton-decoupled ^{13}C spectrum in the F_2 dimension. This allows the multiplicity of the various ^{13}C sites to be determined simply by inspection of the two-dimensional spectrum. More recently, one-dimensional experiments have been proposed that also offer possibilities to determine the multiplicity, but in a more straightforward way.[18–23]

In many cases the use of the conventional two-dimensional *J* spectroscopy experiments leads to practical difficulties. The main problems for the case in which high multiplet resolution is required concern the amount of data storage space needed and the low sensitivity of the experiment in this application. Another problem is that in the proton-flip experiment, which in principle yields the highest multiplet resolution, distortions in the ^{13}C multiplet structure occur if the proton spectrum is not first order. Bodenhausen et al.[59] have demonstrated that accurate values for the heteronuclear coupling constants can still be obtained from such a spectrum, provided that a special two-dimensional simulation program is available.

The so-called "g
tine use and is discu
convenient and mor
of either long-range
discussed in Section

A. The Gated-D

The gated-decouple
the frequencies of t
sketched in Figure
spin echo is created
to the ^{13}C nuclei. D
decoupling is emplo
chemical shift frequ
the evolution period
the ^{13}C magnetizati

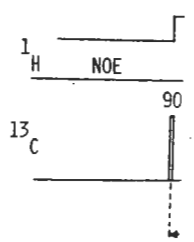

Figure 8.15
Pulse sequence of the
transverse plane for th
and *d* is sketched in F

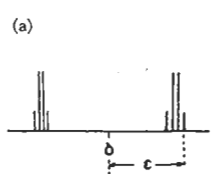

Figure 8.16
(*A*) An arbitrary ^{13}C
component during th
and $\pi\epsilon t_1$, respectivel

The so-called "gated-decoupler" experiment[13–15] is most convenient for routine use and is discussed in Section III.A. Recently, experiments that are more convenient and more sensitive have been proposed for the exact determination of either long-range[74] or direct[75] coupling constants. Those experiments are discussed in Sections III.B and III.C.

A. The Gated-Decoupler Experiment

The gated-decoupler experiment[13–15] is based on modulation of a spin echo with the frequencies of the heteronuclear coupling constants. The pulse sequence is sketched in Figure 8.15. Pertinent diagrams are shown in Figure 8.16. A ^{13}C spin echo is created by means of a $90°_x$–$t_1/2$–$180°_y$–$t_1/2$ pulse sequence, applied to the ^{13}C nuclei. During the first half of the evolution period, broad-band proton decoupling is employed and the transverse ^{13}C magnetization precesses with its chemical shift frequency δ about the z axis (Figure 8.16*b*). At the midpoint of the evolution period, the 180° ^{13}C pulse inverts the angle, $\pi\ \delta\ t_1$, through which the ^{13}C magnetization has precessed (Figure 8.16*c*). During the second half of

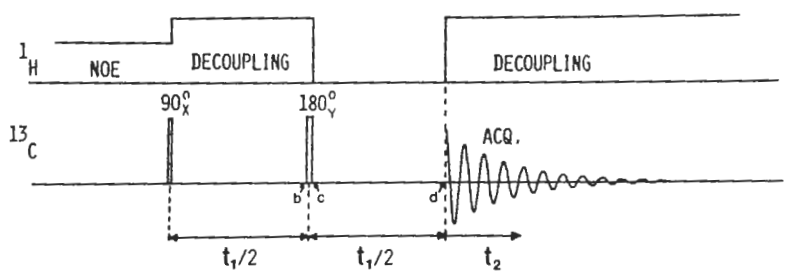

Figure 8.15
Pulse sequence of the gated-decoupler heteronuclear J experiment. The position in the transverse plane for the magnetization of an arbitrary multiplet component at times b, c, and d is sketched in Figure 8.16*b–d*.

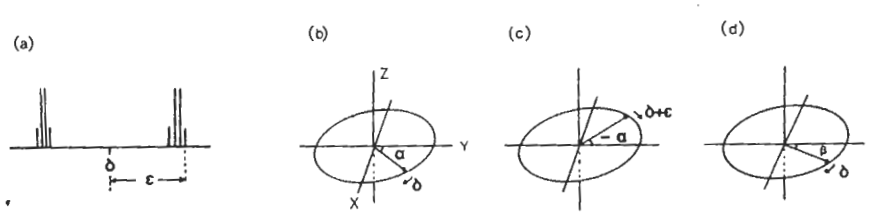

Figure 8.16
(*A*) An arbitrary ^{13}C multiplet structure and (*b–d*) the evolution of a ^{13}C multiplet component during the sequence of Figure 8.15. The angles α and β are equal to $\pi\delta t_1$ and $\pi\epsilon t_1$, respectively.

the evolution period, the magnetization components rotate with frequencies of the resonances in the proton-coupled ^{13}C spectrum. For example, consider a multiplet component at frequency $\delta + \epsilon$, where ϵ is the offset of the resonance considered from the chemical shift frequency δ. This covers an angle $\pi(\delta + \epsilon)t_1$ during the second half of the evolution period. Hence at time t_1, the phase of this specific ^{13}C magnetization component in the transverse plane depends exclusively on the offset from the ^{13}C chemical shift frequency and is given by $\pi\epsilon t_1$. The detected signal is then modulated in phase, as a function of t_1 by $\epsilon/2$, and a two-dimensional Fourier transformation gives a resonance at $(\epsilon/2, \delta)$ if broad-band proton decoupling is employed during acquisition. In a similar way, all other resonances in Figure 8.16*a* induce a resonance in the two-dimensional spectrum on the cross-section $F_2 = \delta$. The normal one-dimensional multiplet pattern will then appear along the F_1 axis on that cross section, even in the case where this pattern is asymmetric due to strong coupling among the protons.[76] Note that all splittings in the F_1 dimension are halved compared with the conventional spectrum; this decreases the obtainable resolution. On the other hand, the effect of static magnetic field inhomogeneity is refocused by the 180° ^{13}C pulse, and therefore inhomogeneity broadening does not appear in the F_1 dimension.

Figure 8.17 shows a gated-decoupler two-dimensional J spectrum of 1 M solution of 5α-androstane in deuteriochloroform, obtained on a Varian XL-200 spectrometer. A 24 × 1024 data matrix was acquired and only one experiment was performed per t_1 value. The total experimental time was 24 × 3 seconds. No attempt was made to resolve the very complex long-range coupling structure. However, for simpler types of molecules this is easily possible.[77,78] In this case one needs fine digitization along the F_1 axis, which generally leads to a very large data matrix. The sensitivity of the experiment decreases fast if the long-range multiplet structure is resolved, because the sensitivity is in the first approximation proportional to the reciprocal of the number of peaks in the two-dimensional spectrum.[79]

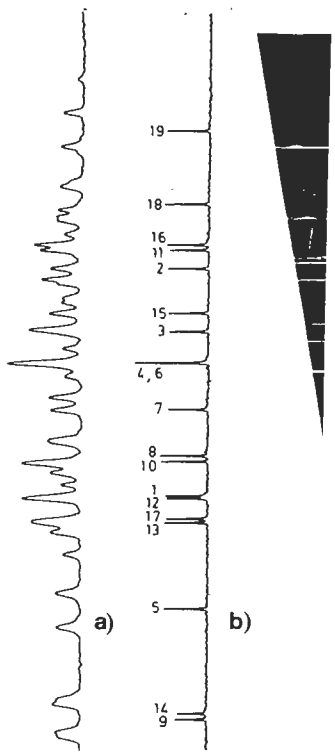

Figure 8.17
The conventional one-dimension
coupled and (*b*) proton decouple
two-dimensional spectrum obtair
76.

B. The Selective Proton-Flip Experiment

As mentioned at the end of the preceding section, both sensitivity and data storage can become a problem if the long-range couplings are studied using the gated-decoupler experiment. A simple way around this problem is the use of the selective proton-flip experiment,[74] which is a modified version of the original proton-flip experiment.[14,15] The pulse sequence is sketched in Figure 8.18. No proton decoupling is applied during the evolution period, but a proton 180° pulse with low rf power (typical rf field strength corresponding to 25 Hz) is applied at the midpoint of the evolution period, in order to invert all resonances of a previously selected proton. Of course this can be done properly only if no

resonances of other protons t
within approximately 125 H

During the first half of the
component, corresponding t
quency $\Omega + \pi J$, where J is
sidered and proton A. Ω is d
coupling to protons other tha

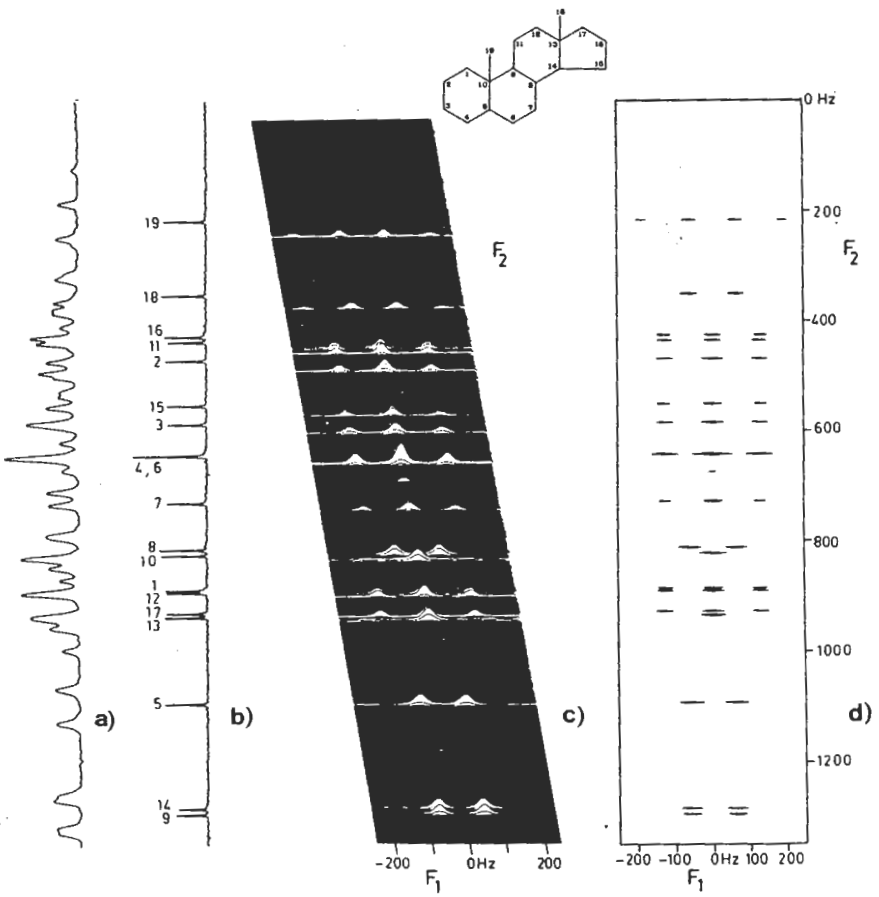

Figure 8.17

The conventional one-dimensional ^{13}C spectra of 5 α-androstane at 50 MHz, (*a*) proton coupled and (*b*) proton decoupled. (*c*) A stacked trace plot and (*d*) a contour plot of the two-dimensional spectrum obtained with the gated-decoupler sequence. From Reference 76.

resonances of other protons that have a coupling to the same ^{13}C site are present within approximately 125 Hz of the resonance selected for inversion.

During the first half of the evolution period in this sequence a certain multiplet component, corresponding to proton A in the α state, rotates with angular frequency $\Omega + \pi J$, where J is the long-range coupling between the carbon considered and proton A. Ω is determined by the ^{13}C chemical shift and the scalar coupling to protons other than A. Just before the 180° ^{13}C pulse, the precession

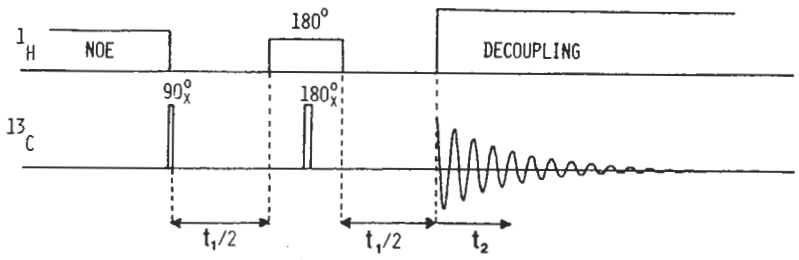

Figure 8.18
Pulse sequence of the selective proton-flip heteronuclear J experiment. The proton transmitter frequency is set to the center of a previously selected proton multiplet, and the proton rf field strength during the semiselective pulse is usually of the order of 25 Hz.

angle through which this ^{13}C magnetization component has evolved equals $(\Omega + \pi J)t_1/2$. The 180° ^{13}C pulse inverts this angle and the selective proton 180° pulse inverts the spin state of proton A. Thus the new frequency of the magnetization component considered is $\Omega - \pi J$. Hence at the end of the evolution period the component has accumulated a total phase equal to $-\pi J t_1$. Similarly, a component starting out with proton A in the β state during the first half of the evolution period will have accumulated a phase $+\pi J t_1$ at the end of the evolution period. During acquisition, broad-band proton decoupling is employed and both components precess with the chemical shift frequency δ. A two-dimensional Fourier transform then gives resonances at $(-J/2, \delta)$ and at $(J/2, \delta)$. Thus all ^{13}C resonances are split in the F_1 dimension by the coupling to proton A. The number of resonances is only doubled compared with the proton-decoupled ^{13}C spectrum, and therefore sensitivity suffers only a factor of 2.[79] The acquisition frequency in the t_1 dimension can be kept low, since only long-range couplings are detected and data storage requirements are minimized.

As an example, Figure 8.19*a* shows the two-dimensional selective J spectrum obtained for the aromatic carbons in a 1 M solution of acetonaphthone (see inset, Figure 8.8a) in acetone-d_6 with selective inversion of proton H1. A 32 × 512 data matrix was acquired, and four experiments were performed for each t_1 value. Some line narrowing was used in the F_1 dimension. Figure 8.19*b* shows phase-sensitive cross sections taken from the spectrum of Figure 8.19*a* at the appropriate ^{13}C chemical shift frequencies. The two-bond coupling to carbon C2 appears to be the only one too small to be measured. As can be seen from the proton spectrum in Figure 8.8a, selective inversion of proton resonances other than H1 is not readily achieved and long-range couplings to those protons cannot straightforwardly be obtained with this method. Again we must realize that the ^{13}C satellites in the proton spectrum should be well enough

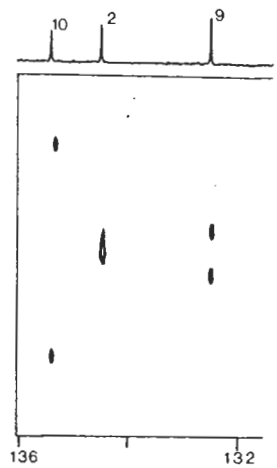

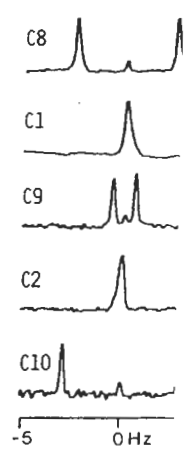

Figure 8.19
(a) Absolute value mode con
acetonaphthone (see inset, F
with selective inversion of pr
dimensional data matrix of (
sites with proton H1.

herence can be used to study the ^{13}C-^{13}C satellites in a proton-decoupled ^{13}C spectra, suppressing the 200-times-stronger signals of isolated ^{13}C nuclei.[41,28] This one-dimensional INADEQUATE experiment can be used to study ^{13}C-^{13}C coupling constants that contain valuable information about the conformation and structure of organic molecules.[85–87] It can also be used for the assignment of ^{13}C resonances by matching the homonuclear ^{13}C coupling constants for the various ^{13}C sites.[88] However, many of the one bond coupling constants have similar magnitudes and the ^{13}C satellites often overlap. A more versatile approach is the measurement, via a two-dimensional experiment, of the double quantum frequency for coupled ^{13}C pairs, which will, of course, show the same double quantum frequency. In Section IV.D this two-dimensional double quantum INADEQUATE experiment is discussed.

In order to facilitate understanding the two-dimensional INADEQUATE experiment, first the original one-dimensional version is discussed. The basis of the idea is that in the rare case that a molecule contains two coupled ^{13}C nuclei, it is possible to generate a double quantum coherence.

A. Double Quantum Coherence

In this section, the phenomenon of double quantum coherence and its phase properties are discussed briefly.

In the case of an isolated ^{13}C nucleus under conditions of continuous broadband proton decoupling, the energy level diagram is given in Figure 8.22*a*. In the case of two coupled ^{13}C nuclei the energy level diagram of Figure 8.22*b* is appropriate. It is obvious from those diagrams that only in a case of such as Figure 8.22*b* can a double quantum transition (here called double quantum coherence) be generated. The wave function, ψ, of the coupled spin system is always a linear combination of eigenfunctions:

$$\psi = c_1|\alpha\alpha\rangle + c_2|\alpha\beta\rangle + c_3|\beta\alpha\rangle + c_4|\beta\beta\rangle \tag{2}$$

Magnetization along the x axis of the rotating frame, M_x, is given by

$$M_x = C\,\overline{\langle\psi|F_x|\psi\rangle} \tag{3}$$

where C is a constant, F_x equals $I_{x_1} + I_{x_2}$, I_{x_1} equals $(I_{+1_1} + I_{-1_1})/2$, and the subscripts 1 and 2 denote the two carbons. Substitution of Equation 2 in Equation 3 and averaging over the entire sample gives

$$M_x = \frac{C}{2}\,\overline{(c_1^*c_2 + c_1c_2^* + c_1^*c_3 + c_1c_3^* + c_2^*c_4 + c_2c_4^* + c_3^*c_4 + c_3c_4^*)} \tag{4}$$

where c_1^* denotes the complex
and can be written as

Transverse magnetization bet

and

that is, if coherence exists b
is generally called phase col
these two specific states this
larly, if a state with $c_1c_4^* \neq$
coherence, for the total magr
two eigenstates. It can be sho
that a $90°_x$–$1/(4J)$–$180°_x$–$1/(4J$
longitudinal magnetization is
a single 90° pulse converts a
coherence. At time Δ in the
have a situation in which all
coupling close to the value J
quantum coherence. Of cou
for isolated ^{13}C nuclei.

B. Selecting Signals Ori

The trick of the INADEQU
double quantum coherence[81,
tum coherence exclusively
shown[73,81,82,48] that if the fin

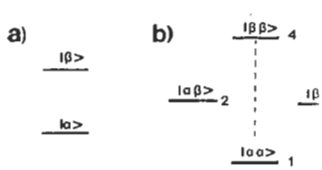

where c_1^* denotes the complex conjugated value of c_1. The element c_1 is complex and can be written as

$$c_1 = |c_1| \exp(i\alpha_1) \tag{5}$$

Transverse magnetization between levels 1 and 2 is present if

$$\overline{|c_1| \times |c_2|} \neq 0 \tag{6a}$$

and

$$\overline{\exp(i\alpha_1 - i\alpha_2)} \neq 0 \tag{6b}$$

that is, if coherence exists between the two phases α_1 and α_2. This condition is generally called phase coherence between levels 1 and 2. For the case of these two specific states this is referred to as single quantum coherence. Similarly, if a state with $c_1 c_4^* \neq 0$ is created, this is a so-called double quantum coherence, for the total magnetic quantum number differs by two units for the two eigenstates. It can be shown explicitly,[89] using the density matrix formalism, that a 90°_x–$1/(4J)$–180°_x–$1/(4J)$ 90°_x pulse sequence creates a state in which all longitudinal magnetization is converted into double quantum coherence, just as a single 90° pulse converts all longitudinal magnetization into single quantum coherence. At time Δ in the pulse sequence sketched in Figure 8.23, we thus have a situation in which all molecules that have two ^{13}C nuclei with a mutual coupling close to the value J (selected in generating the sequence), have double quantum coherence. Of course, no double quantum coherence can be created for isolated ^{13}C nuclei.

B. Selecting Signals Originating from Double Quantum Coherence

The trick of the INADEQUATE experiment is to use the phase properties of double quantum coherence[81,82] to select signals that originate from double quantum coherence exclusively when another 90° pulse is applied. It can be shown[73,81,82,48] that if the final pulse is applied along the y axis instead of along

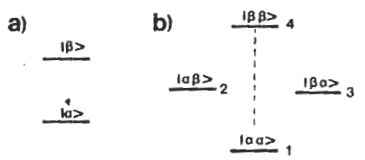

Figure 8.22
Energy level diagram for ^{13}C in the case of (*a*) an isolated ^{13}C and (*b*) homonuclear coupled ^{13}C nuclei. Only in the latter case can a double quantum coherence (broken line) be created.

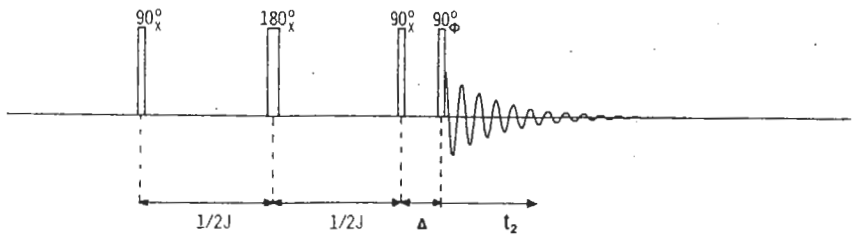

Figure 8.23
Pulse sequence of the one-dimensional INADEQUATE experiment. The phases of the final read pulse and of the receiver[55] are cycled according to Table 8.3. The delay Δ is very short (2 μsec) and is necessary on most spectrometers to allow rf phase shifting. Proton decoupling is employed throughout.

the x axis, this is felt by the double quantum coherence as a phase shift by 180° instead of by 90°. If four experiments are performed with four different phases of the final "read pulse," and the signals are co-added with a receiver reference phase,[55] as given in Table 8.3, and chosen to follow the transverse magnetization originating from the double quantum coherence present during the time Δ, then only signals from the molecules with two coupled ^{13}C nuclei are present in the sum of the detected signals. The phases of the magnetization components during detection, originating from longitudinal and transverse magnetization during the time Δ, are also given in Table 8.3. As can be seen from this table, in the sum of the results of the four experiments, no signal is present that originates from longitudinal magnetization or single quantum coherence during the time Δ.

Table 8.3
Phase of the Detection Pulse, ϕ, and the Receiver Reference Phase,[55] ψ, Compared with the Three Components Originating from Longitudinal Magnetization (LM), Single Quantum Coherence (SQ), and Double Quantum Coherence (DQ), Immediately After the Detection Pulse, in the Scheme Sketched in Figure 8.23

ϕ	LM	SQ	DQ[a]	ψ
x	$-y$	x	x	x
y	x	y	$-y$	$-y$
$-x$	y	x	$-x$	$-x$
$-y$	$-x$	y	y	y

[a]Phase of one of the two doublet components; the other component always starts out with opposite phase.

C. Experimental Conside

1. Further Phase Cycling

The phase cycling given in unwanted signals. In practice 90° (e.g., between the x and signals from isolated ^{13}C nuc mogeneity, off-resonance eff tudes of the various phase s isolated ^{13}C signals in the four of 20. Much better suppressi four step experiment is emplo

The following extensions used:

1. The entire four step e pulses and of the rece 16-step experiment. T CLOPS cycling usec ments.[62]
2. The phase of the firs inverted as well. This
3. The phase of the 18 provided that the rec 180° pulse is increme experiment.

For the two-dimensional I wanted signals appears to be if long-range couplings are s sufficient, and often one doe

2. Optimizing Sensitivit

Of course, in this type of e results in a sensitivity that conventional proton-decoupl to use sample concentratior reported on sucrose[45] were centration. It is always nece to the transverse decay tim experiment this can lead to data storage space needed;

C. Experimental Considerations

1. Further Phase Cycling

The phase cycling given in Table 8.3 suggests a perfect suppression of all unwanted signals. In practice, however, the rf phase shifts will not be exactly 90° (e.g., between the x and the y axes), and nonperfect cancellation of the signals from isolated ^{13}C nuclei occurs. Other nonidealities are due to rf inhomogeneity, off-resonance effects, and the sometimes slightly different amplitudes of the various phase shifted pulses. Therefore, the suppression of the isolated ^{13}C signals in the four step experiment often is only a factor of the order of 20. Much better suppression can be obtained if further phase cycling of the four step experiment is employed.[48]

The following extensions of the phase cycling given in Table 8.3 can be used:

1. The entire four step experiment is repeated four times with phases of all pulses and of the receiver[55] incremented by 90° each time, leading to a 16-step experiment. This extra phase cycling is analogous to the CYCLOPS cycling used in conventional one-dimensional nmr experiments.[62]
2. The phase of the first pulse can be inverted if the receiver phase is inverted as well. This extends the experiment to a 32 step sequence.
3. The phase of the 180° pulse can be cycled through all four phases, provided that the receiver phase is inverted each time the phase of the 180° pulse is incremented by 90°. This finally gives rise to a 128 step experiment.

For the two-dimensional INADEQUATE experiment, suppression of the unwanted signals appears to be not as critical as in the one-dimensional version if long-range couplings are studied. A suppression factor of 50–100 is usually sufficient, and often one does not need the full 128 step sequence.

2. Optimizing Sensitivity

Of course, in this type of experiment one detects only the ^{13}C satellites; this results in a sensitivity that is a factor of about 200 lower than that of the conventional proton-decoupled ^{13}C spectrum. Therefore, it is important always to use sample concentrations as high as possible. For example, experiments reported on sucrose[45] were performed at 70°C in order to allow a higher concentration. It is always necessary to accumulate signal for a time at least equal to the transverse decay time (T_2) of the ^{13}C signal. In the two-dimensional experiment this can lead to a requirement of an exceedingly large amount of data storage space needed; thus it can be useful to employ a relaxation agent,

which shortens the required acquisition time and in the mean time increases the repetition rate of the experiment by shortening the ^{13}C T_1's. A usually better option in the case of long ^{13}C T_1's (>3 sec) is to use the INEPT-INADEQUATE version of the experiment,[90] possibly in combination with a small amount of relaxation agent. In the normal INADEQUATE experiments (either one- or two-dimensional), optimum sensitivity is obtained if the time between the last 90° pulse of one experiment and the first 90° pulse of the next experiment is equal to $1.3T_1$,[63] where T_1 is the average longitudinal relaxation time of the protonated carbons. Signals from coupled pairs of protonated and quaternary carbons then show only about half the intensity, and pairs of coupled quaternary carbons show very low intensity. In the case where the INEPT version is used,[90] the delay time between the end of acquisition and the first 90° ^{13}C pulse must be $1.3\,T_1$, where T_1 is now the average longitudinal relaxation time of the protons.

D. Shift Correlation of Coupled ^{13}C Nuclei

The possibility of suppressing the signals from isolated ^{13}C nuclei allows the application of homonuclear shift correlation techniques on the satellite signals. This is most easily accomplished by measuring the double quantum frequency for the various ^{13}C sites. Two coupled ^{13}C nuclei show the same double quantum frequency, which is equal to the sum of the corresponding chemical shift offset frequencies from the ^{13}C transmitter frequency. If the time Δ, during which the double quantum coherence is present, is converted into the variable evolution period, t_1, the detected satellite signals are modulated as a function of t_1 with the frequency of the double quantum coherence.[48] Coupled ^{13}C nuclei can then be identified because they show an identical double quantum modulation frequency. The value of the delays, $1/(4J)$, in the double quantum excitation sequence is usually set to 6 msec, so that double quantum coherence is generated only for directly coupled ^{13}C nuclei.

It can be shown that the detected satellite signals are modulated in amplitude with the double quantum frequencies.[48] However, amplitude modulation does not allow the determination of the sign of the double quantum frequencies, which can, in some cases, lead to ambiguities. In order to allow determination of the sign of the double quantum frequency, the detected signals must be modulated in phase. This can be accomplished by adding the results of a complementary experiment in which a composite 45° pulse along the z axis is applied during the evolution period.[45,91] A simpler and more sensitive alternative is to change the width of the final read pulse to correspond to either 50° or 130°. This directly generates satellite signals that are mainly phase modulated as a function of t_1 and that have a 25% larger amplitude.[46] The theory of this mechanism is rather complicated and requires either the use of the density matrix formalism or the use of fictitious spin-$\frac{1}{2}$ operators.[82,92,94] It can be shown that in the case of an inhomogeneous static magnetic field, a read pulse with a flip angle of 130°

gives slightly better sens
image signals in the F_1
quantum frequency. Tho
signals, and usually do n

As an example, Fi
the alkaloid panamine, o

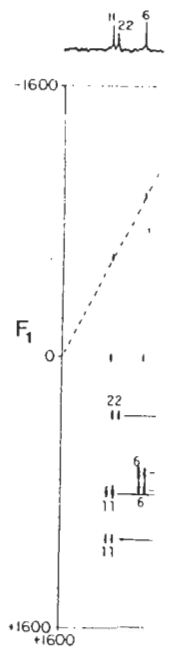

Figure 8.24
Carbon-carbon connectivit
ination of the double qua
quantum frequencies for c
onal", $F_1 = 2F_2$, which
quency and the double qua
was kindly provided by Dr

on a Varian XL200 spectrometer. A sample concentration of approximately 2.5 M in deuteriochloroform was used, and the total measuring time was 10 hr. 512 experiments were performed for each t_1 value and a 64 × 1024 data matrix was aquired. The identical double quantum frequencies for pairs of coupled ^{13}C nuclei are clearly visible in Figure 8.24, and are connected by the drawn lines. Because the double quantum frequency equals the sum of the single quantum frequencies, the centers of the drawn lines are on the "diagonal," $F_1 = 2F_2$, which is indicated by the broken line. The spectral width in the F_1 dimension was chosen smaller than twice the spectral width in the F_2 dimension, in order to save data storage space, and the "diagonal" is folded, as are the double quantum frequencies for the pairs C19, C20 and C20, C21. Even the quaternary carbon (C9) shows double quantum frequencies for all four bonded carbons. The only linkages not detected by the experiment were those between the strongly coupled pairs C15, C16 and C3, C4. This is because for strongly coupled spins the condition for creating double quantum coherence is different from that of the weakly coupled cases.[42] Some contours of spurious signals are also visible in this spectrum. Those are due to incompletely suppressed signals from isolated ^{13}C nuclei.

It is clear from this example that a ^{13}C double quantum spectrum, possibly in combination with multiplicity determination,[18–23] makes it possible to reconstruct almost the complete ^{13}C skeleton of organic molecules. Some impressive examples of the use of the experiment have already appeared in the literature.[47,94,95] High-field spectrometers are presently available that offer sensitivity that is much better than for the 200 MHz spectrometer on which the spectrum of Figure 8.24 was recorded. High sensitivity makes routine use of ^{13}C double quantum spectroscopy feasible, and the method might become a widely applied technique.

ACKNOWLEDGMENTS

The author gratefully acknowledges many valuable suggestions and comments from Prof. G. E. Maciel in the preparation of the manuscript. Discussions with Drs. R. Freeman, A. F. Mehlkopf, and Prof. J. Smidt were essential for writing this chapter. The author is indebted to Dr. T. Mareci for sending the double quantum ^{13}C spectrum of panamine, to Dr. B. Hawkins for technical assistance, and to Drs. P. H. Bolton and S. L. Patt for sending preprints and other unpublished material. This work was supported by a grant from the U.S. Department of Energy (Laramie Energy Technology Center). Experiments were performed at the Colorado State Regional NMR Center, supported by National Science Foundation Grant No. CHE 78–18581.

REFERENCES

1. R. R. Ernst and W. A. A
2. V. Royden, *Phys Rev.* **9**
3. R. R. Ernst, *J. Chem. P*
4. J. B. Grutzner and A. E.
5. M. H. Levitt and R. Free
6. J. S. Waugh, *J. Magn. R*
7. A. Abragam, *The Princ* Press, London, 1961, (
8. E. B. Baker, *J. Chem. P*
9. W. A. Anderson and F. *A*
10. J. Jeener, Ampere Interna 1971.
11. W. P. Aue, E. Bartholdi, *a*
12. L. Muller, A. Kumar, an
13. G. Bodenhausen, R. Free (1976).
14. G. Bodenhausen, R. Freen *Resonance* **24,** 291 (19
15. A. Kumar, W. P. Aue, F Ernst, Proc. XIXth con
16. P. Bachmann, W. P. Aue, **28,** 29 (1977).
17. G. A. Morris and R. Free
18. M. H. Levitt and R. Freer
19. D. P. Burum and R. R. E
20. D. M. Doddrell and D. T.
21. F. K. Pei and R. Freeman
22. D. M. Doddrell, D. T. Pe 323 (1982).
23. H. Jakobsen, O. Sorensen *nance* **48,** 328 (1982).
24. H. Gunther, H. Seel, and (1977).
25. A. A. Maudsley and R. R.
26. A. A. Maudsley, L. Muller (1977).

REFERENCES

1. R. R. Ernst and W. A. Anderson, *Rev. Sci. Instr.* **37,** 93 (1966).
2. V. Royden, *Phys Rev.* **93,** 944 (1954).
3. R. R. Ernst, *J. Chem. Phys.* **45,** 3845 (1966).
4. J. B. Grutzner and A. E. Santini, *J. Magn. Resonance* **19,** 178 (1975).
5. M. H. Levitt and R. Freeman, *J. Magn. Resonance* **43,** 502 (1981).
6. J. S. Waugh, *J. Magn. Resonance* **50,** 30 (1982).
7. A. Abragam, *The Principles of Nuclear Magnetism,* Oxford University Press, London, 1961, Chapter 8.
8. E. B. Baker, *J. Chem. Phys.* **37,** 911 (1962).
9. W. A. Anderson and F. A. Nelson, *J. Chem. Phys.* **39,** 183 (1963).
10. J. Jeener, Ampere International Summer School, Basko Polje, Yugoslavia, 1971.
11. W. P. Aue, E. Bartholdi, and R. R. Ernst, *J. Chem. Phys.* **64,** 2229 (1976).
12. L. Muller, A. Kumar, and R. R. Ernst, *J. Chem. Phys.* **63,** 5490 (1975).
13. G. Bodenhausen, R. Freeman, and D. L. Turner, *J. Chem. Phys.* **65,** 839 (1976).
14. G. Bodenhausen, R. Freeman, R. Niedermeyer, and D. L. Turner, *J. Magn. Resonance* **24,** 291 (1976).
15. A. Kumar, W. P. Aue, P. Bachmann, J. Karhan, L. Muller, and R. R. Ernst, Proc. XIXth congress Ampere, Heidelberg, 1976.
16. P. Bachmann, W. P. Aue, L. Muller, and R. R. Ernst, *J. Magn. Resonance* **28,** 29 (1977).
17. G. A. Morris and R. Freeman, *J. Magn. Resonance* **29,** 433 (1978).
18. M. H. Levitt and R. Freeman, *J. Magn. Resonance* **39,** 533 (1980).
19. D. P. Burum and R. R. Ernst, *J. Magn. Resonance* **39,** 163 (1980).
20. D. M. Doddrell and D. T. Pegg, *J. Am. Chem. Soc.* **102,** 6388 (1980).
21. F. K. Pei and R. Freeman, *J. Magn. Resonance* **48,** 318 (1982).
22. D. M. Doddrell, D. T. Pegg, and M. R. Bendall, *J. Magn. Resonance* **48,** 323 (1982).
23. H. Jakobsen, O. Sorensen, W. S. Brey, and P. Kanyha, *J. Magn. Resonance* **48,** 328 (1982).
24. H. Gunther, H. Seel, and H. Schmickler, *J. Magn. Resonance* **28,** 145 (1977).
25. A. A. Maudsley and R. R. Ernst, *Chem. Phys. Lett.* **50,** 368 (1977).
26. A. A. Maudsley, L. Muller, and R. R. Ernst, *J. Magn. Resonance* **28,** 463 (1977).

27. G. Bodenhausen and R. Freeman, *J. Magn. Resonance* **28,** 471 (1977).
28. R. Freeman, *Proc. R. Soc. London A* **373,** 149 (1980).
29. L. Muller, *J. Am. Chem. Soc.* **101,** 4481 (1979).
30. A. Minoretti, W. P. Aue, M. Reinhold, and R. R. Ernst, *J. Magn. Resonance* **40,** 175 (1980).
31. A. Bax and G. A. Morris, *J. Magn. Resonance* **42,** 501 (1981).
32. M. R. Bendall, D. T. Pegg, D. M. Doddrell, and D. M. Thomas, *J. Magn. Resonance* **46,** 43 (1982).
33. J. Jeener, B. H. Meier, P. Bachmann, and R. R. Ernst, *J. Chem. Phys.* **71,** 4546 (1979).
34. B. H. Meier and R. R. Ernst, *J. Am. Chem. Soc.* **101,** 6441 (1979).
35. Y. Huang, S. Macura, and R. R. Ernst, *J. Am. Chem. Soc.* **103,** 5327 (1981).
36. Y. Huang, G. Bodenhausen, and R. R. Ernst, *J. Am. Chem. Soc.* **103,** 6989 (1981).
37. G. Bodenhausen and R. R. Ernst, *Mol. Phys.* **47,** 319 (1982).
38. S. Forsen and R. A. Hoffmann, *J. Chem. Phys.* **39,** 2892 (1963).
39. S. Forsen and R. A. Hoffmann, *J. Chem. Phys.* **40,** 1189 (1964).
40. S. Forsen and R. A. Hoffman, *J. Chem. Phys.* **45,** 2049 (1966).
41. A. Bax, S. P. Kempsell, and R. Freeman, *J. Am. Chem. Soc.* **102,** 4849 (1980).
42. A. Bax and R. Freeman, *J. Magn. Resonance* **41,** 507 (1980).
43. A. Bax, R. Freeman, and S. P. Kempsell, *J. Magn. Resonance* **41,** 349 (1980).
44. A. Bax, R. Freeman, and T. A. Frenkiel, *J. Am. Chem. Soc.* **103,** 2102 (1981).
45. A. Bax, R. Freeman, T. A. Frenkiel, and M. H. Levitt, *J. Magn. Resonance* **44,** 409 (1981).
46. T. H. Mareci and R. Freeman, *J. Magn. Resonance* **48,** 158 (1982).
47. R. Freeman, T. A. Frenkiel, and M. B. Rubin, *J. Am. Chem. Soc.* **104,** 5545 (1982).
48. A. Bax, *Two-dimensional Nuclear Magnetic Resonance in Liquids,* Reidel, Boston, 1982, Chapter 5.
49. G. A. Morris and R. Freeman, *J. Am. Chem. Soc.* **101,** 760 (1979).
50. G. A. Morris, Chapter 7 of this book.
51. G. Bodenhausen and D. J. Ruben, *Chem. Phys. Lett.* **69,** 185 (1980).
52. P. H. Bolton, *J. Magn. Resonance* **48,** 336 (1982).
53. Of course, the modula
resonances from the
54. Reference 48, Chapter
55. In practice, it is not the
in the computer of t
has the same effect
have had.
56. N. J. Clayden, F. Inag
Tokura, and T. Miy
57. T. M. Chan and J. L.
58. Note that those proton
the conventional pro
59. G. Bodenhausen, R. F
Resonance **28,** 17 (1
60. J. Keeler, Part II thesi
61. P. H. Bolton, *J. Magn*
62. D. I. Hoult and R. E. I
63. J. S. Waugh, *J. Mol.*
64. A. Bax, *J. Magn. Res*
65. M. H. Levitt, private
66. A. Bax, A. F. Mehlk
(1979).
67. G. Wagner, K. Wuth
(1978).
68. I. D. Campbell, C. M
Magn. Resonance 1
69. A. Bax, R. Freeman,
(1981).
70. A. G. Ferrige and J. C
71. P. H. Bolton and G. E
72. A. Bax, *J. Magn. Res*
73. G. Bodenhausen, *Prog*
74. A. Bax and R. Freem
75. A. Bax, *J. Magn. Res*
76. Reference 48, Chapter
77. R. Freeman, G. A. Mo
(1979).

78. L. D. Hall, G. A. Morris, and S. Sukumar, *Carbohydr. Res.* **76,** C7 (1979).
79. W. P. Aue, P. Bachmann, A. Wokaun, and R. R. Ernst, *J. Magn. Resonance* **29,** 523 (1978).
80. H. Hatanaka, T. Terao, and T. Hashi, *J. Phys. Soc. Japan* **39,** 835 (1975).
81. A. Wokaun and R. R. Ernst, *Chem. Phys. Lett.* **52,** 407 (1977).
82. A. Wokaun, Doctoral Thesis, Zurich, 1978.
83. A. Wokaun and R. R. Ernst, *Mol. Phys.* **36,** 317 (1978).
84. W. S. Warren, S. Sinton, D. P. Weitekamp, and A. Pines, *Phys. Rev. Lett.* **43,** 1791 (1979).
85. G. E. Maciel, *NMR Spectroscopy of Nuclei other than Protons,* T. Axenrod and G. A. Webb, Eds., Wiley-Interscience, New York, 1974, Chapter 13.
86. V. F. Bystrov, *Prog. NMR Spectrosc.* **10,** 41 (1976).
87. P. E. Hansen, *Org. Magn. Resonance* **11,** 215 (1978).
88. R. Richarz, W. Amman, and T. Wirthlin, *J. Magn. Resonance* **45,** 270 (1981).
89. Reference 48, Appendix 1.
90. O. W. Sorensen, R. Freeman, T. A. Frenkiel, T. H. Mareci, and R. Schuck, *J. Magn. Resonance* **46,** 180 (1982).
91. R. Freeman, T. A. Frenkiel, and M. H. Levitt, *J. Magn. Resonance* **44,** 409 (1981).
92. A. Wokaun and R. R. Ernst, *J. Chem. Phys.* **68,** 5518 (1978).
93. S. Vega and A. Pines, *J. Chem. Phys.* **66,** 5624 (1977).
94. J. A. Robinson and D. L. Turner, *J. Chem. Soc. Chem. Commun.* 148 (1982).
95. F. J. Schmitz, S. K. Agarwal, S. P. Gunasekera, P. G. Schmidt and J. N. Shoolerey, *J Am. Chem. Soc.* **105,** 4835 (1983).

9 FACTOR
ACCURA
LATTICE
MEASUI

DAVID J. CRAI
GEORGE C. LE

CONTENTS